STRUCTURE AND APPEARANCE OF ENVELOPES AROUND PROTOSTARS

Harold W. Yorke
Max-Planck-Institut für Physik und Astrophysik,
Föhringer Ring 6, 8000 München 40, FRG.

I. Introduction - An overall picture of star formation

The existence of material in the immediate vicinity of young main sequence stars or even younger objects, protostars, still contracting and evolving towards the main sequence, is related closely to the details of star formation. Although a number of individual idealized problems related to star formation have been well studied, our overall understanding of how interstellar matter evolves into full fledged hydrogen-burning stars can be deemed qualitative at best. The emerging picture is neither complete nor should it be considered the final answer as to how stars form. Let us summarize this picture by a list of "axioms", valid for star formation (SF) in the plane of our Galaxy.

SF 1 Stars form preferentially in spiral arms.

The concentration of giant HII regions and O-B associations in recognizable spiral patterns requires that the regions of active star formation and the regions favourable to such be close by. SF 1 seems readily explainable (at least qualitatively) by the density wave theory of spiral structure developed by Lin and associates (see eg. Lin, 1971). A rotating disk of gas and stars develops ripples or waves in a coherent pattern which move relative to the gas. Interstellar matter flowing into these density waves is compressed, thus enhancing the probability of star formation - either by initiating a phase transition in the hot component of the interstellar gas ($T \sim 10^4$ K) whereby cold clouds ($T \sim 10^2$ K) are produced and/or existing clouds grow in mass (Biermann et al., 1972), or by simply increasing the density of existing clouds (Shu et al., 1972). Some of these clouds become gravitationally unstable; the ensuing collapse results in stars.

SF 2 Stars condense out of large molecular clouds ($M \gtrsim 10^4 M_\odot$).

SF 2 explains why infrared sources of colour temperatures less than

https://doi.org/10.1017/S0252921100069165 Published online by Cambridge University Press

100 K to 1000 K and of luminosities from 10^2 $L_\odot$ to 10^5 $L_\odot$ are found imbedded in dense molecular cloud complexes. Often correlated both with the positions of compact HII regions (Wynn-Williams and Becklin, 1974; Brown and Zuckerman, 1975) and with OH and H_2O masering spots, such infrared hot spots are to be interpreted as massive protostars or early type main sequence stars surrounded by dusty shells (Yorke, 1977). SF 2 also explains why stars tend to form in localized groups (associations).

SF 3 A gravitationally unstable cloud will fragment into a number of smaller mass concentrations.

A cloud starts to collapse when the gravitational forces of attraction overcome the combined forces of internal gas pressure, magnetic fields, turbulence and rotation. Considering the gravitational binding energy and the thermal kinetic energy only, one obtains minimal requirements to be satisfied in order to allow a gas cloud to collapse gravitationally (Jeans criterion):

$$\frac{M}{[10^3\ M_\odot]} \gtrsim \left(\frac{T}{[60\ K]}\right)^{3/2} \left(\frac{n_H}{[10\ cm^{-3}]}\right)^{-1/2} \qquad (1)$$

For the temperatures T and hydrogen number densities n_H found in typical interstellar clouds, the smallest unstable mass M is of the order of 10^3 $M_\odot$. For the dense molecular clouds of SF 2, however, the Jeans criterion is fulfilled by several orders of magnitude (ignoring magnetic fields, turbulence and rotation). There is also a minimum time scale for gravitational collapse. Ignoring now the internal gas pressure and considering only gravity, one can calculate the free fall time scale t_{ff} of a collapsing cloud:

$$\frac{t_{ff}}{[2.1\ 10^5\ y]} = \left(\frac{\rho}{[10^{-19} g\ cm^{-3}]}\right)^{-1/2} \qquad (2)$$

where ρ is the gas density. Thus, although equation (1) tells us that dense, massive molecular clouds my be collapsing gravitationally, equation (2) indicates that this collapse should proceed non-homologously. If the original cloud were to be somewhat clumpy initially, each of the higher density clumps (or fragments) satisfying the Jeans criterion will collapse more or less independently on a shorter time scale than the original cloud. The process of fragmentation is responsible for the fact that stars of masses between ~0.1 $M_\odot$ and ~60 $M_\odot$, rather than 10^3 $M_\odot$ stars, are formed in molecular clouds.

https://doi.org/10.1017/S0252921100069165 Published online by Cambridge University Press

The process of fragmentation continues until the smallest fragments, the protostellar clouds which later evolve into stars, are produced. In some cases fragmentation stops at less than 1 $M_\odot$ and in other cases a more massive protostellar cloud of say 20 $M_\odot$ or 50 $M_\odot$ is formed. Why is this, Certainly optical depth effects, thermal behaviour of the gas and the tidal forces from the already existing clumps play a major role. Understanding the details of fragmentation is crucial to the understanding of such long-standing problems as the initial stellar mass spectrum and the rate of star formation. Since, however, the dynamics of collapse and fragmentation are sensitive to the presence of turbulence, magnetic fields and large scale gas flows as well as the detailed thermal and radiative properties of the dusty molecular gas, numerical calculations of this problem have always had to be rather crude, refering to idealized special cases only. The interested reader is refered to Larson's (1977) review and the references therein.

SF 4 The smallest fragment, the protostellar cloud, collapses non-homologously.

The basic features of the evolution of the final fragment, the protostellar cloud , have been discussed extensively in the literature (see for instance the reviews given by Larson, 1973; Larson, 1977; Kippenhahn and Tscharnuter, 1975). In spite of large differences in the initial conditions and assumptions adopted by various authors, the results of different numerical collapse calculations are at least qualitatively similar. In all cases the collapse proceeds non-homologously; the central regions of the protostellar cloud collapse most rapidly and there is a runaway increase in the central density. The reason for this highly non-uniform increase is twofold: 1.) according to equation (2) the densest regions have a shorter free fall time scale and should therefore collapse the fastest; and 2.) the collapse in the outer regions of the cloud is retarded by pressure gradients. Even if the density distribution is uniform initially, pressure gradients soon develop as the material available for collapse is exhausted in the outer regions.

When the central condensation becomes optically thick it can no longer cool effectively. The central temperature rises sharply, pressure gradients build up and for a small star-like core the free fall is stopped. If this core consists of molecular hydrogen, the material can again begin to collapse in almost free fall when the hydrogen

dissociates. The second optically opaque core which then forms is the embryo star. It contains only a fraction of the original mass of the protostellar cloud. Because the core is in approximate hydrostatic equilibrium in its interior, it is in many respects similar to a star. Its internal energy source arises from the (slow) gravitational contraction on a Kelvin-Helmholtz time scale t_{KH}

$$\frac{t_{KH}}{[3\times10^{7}y]} \approx \left(\frac{M_{core}}{[M_{\odot}]}\right)^{2} \left(\frac{R_{core}}{[R_{\odot}]}\right)^{-1} \left(\frac{L_{core}}{[L_{\odot}]}\right)^{-1} \qquad (3)$$

where M_{core} is the core mass, R_{core} the core radius, L_{core} the intrinsic core luminosity. At the same time the core is contracting and evolving towards the main sequence, material in the surrounding envelope still falls onto the core at approximately free fall velocities. The infall velocity is supersonic and consequently a shock front forms above the surface of the protostar, where the kinetic energy of the material accreting onto the star is converted into thermal energy. In a geometrically thin region (relaxation zone) located between the shock front and the core surface much of this thermal energy is radiated away and the newly accreted material can settle onto the core. Figure 1 displays schematically the temperature distribution in the vicinity of the accretion shock front. These results for a collapsing one solar mass protostellar cloud were taken from Winkler (1977), who did not rely on "artificial viscosity" to smear out the shock front. The magnitude of the luminosity L_{shock} emitted from this relaxation zone is of the order:

$$L_{shock} \approx \frac{GM_{core}}{R_{core}} \dot{M} \qquad (4)$$

where $\dot{M}$ is the rate of mass accretion onto the core.

The non-homologous collapse as described in the previous paragraphs has important theoretical and observational consequences. Due to the combined effects of the intrinsic core luminosity and the heat radiated away at the accretion shock front, a newly formed protostar is quite luminous long before it reaches the main sequence. Because, however, the core and accretion shock front are completely obscured optically by the infalling dusty material, the protostar can be observed only indirectly in the radio, microwave and infrared regions of the spectrum by its effect on its immediate surroundings. Examples of such interactions are: 1.) compact HII regions where H and He are ionized in a region the size of the original protostellar

https://doi.org/10.1017/S0252921100069165 Published online by Cambridge University Press

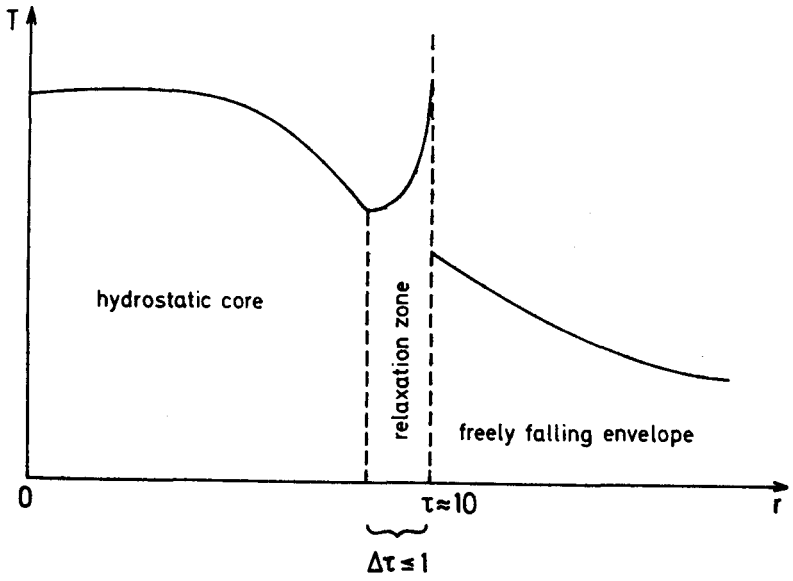

Fig. 1. The temperature distribution in the vicinity of the shock front surrounding an accreting protostar is displayed schematically. Note the pre-heating of material in the freely falling envelope, the overshoot at the discontinuous shock and the relaxation zone, where the heat is radiated away. This schematic diagram was taken from Tscharnuter, 1976 by permission of author.

https://doi.org/10.1017/S0252921100069165 Published online by Cambridge University Press

cloud; 2.) C^+ regions, where C is ionized but H and He are not; 3.) "hot spots" in molecular clouds of enhanced molecular line radiation, probably due to collisions with warm ($T \sim 100$ K) dust grains; 4.) H_2O, OH and SiO maser sources; 5.) line profiles and dust absorption features (combined emission and absorption); and 6.) infrared continuum radiation from dust heated by protostellar radiation and from free-bound emission. Only after most of the material in the envelope has either accreted onto the star or has been dispersed by radiation pressure and/or by a stellar wind can the protostar or young main sequence star be observed optically.

In the following we wish to describe the structure and appearance of envelopes around protostars during the various evolutionary phases up to the time at which the central source becomes visible optically.

II. Spherical Collapse

a.) "Massive" versus "low mass" protostars.

For several reasons it is convenient to distinguish between the evolution of "massive" ($M \gtrsim 3\ M_\odot$) and "low mass" ($M \lesssim 1\ M_\odot$) protostars and their envelopes. The basic differences are summarized as follows:

1. Compared to the accretion time scale $t_{acc} = M_{core}/\dot{M}$, the low mass protostellar core evolves rather slowly. When the low mass protostar first becomes optically visible, it is located near the lower end of its Hayashi track. It can contract only as fast as it transports energy from the interior to the surface and then radiates it away. Its final pre-main sequence evolution is governed by the Kelvin-Helmholtz time scale, equation (3). The more massive protostellar core, on the other hand, starts burning hydrogen before the accretion process stops and while a significant fraction of the mass is still in the obscuring infalling envelope. Thus, for part of its main sequence lifetime, the massive protostar should not be visible optically.

2. Massive protostars cannot accrete all of the material in the original protostellar cloud - even in the most favourable case of no rotation, no turbulence, no magnetic fields - due to a variety of effects. According to Appenzeller and Tscharnuter (1974) the rapid compression of the protostellar core could lead to an overproduction

https://doi.org/10.1017/S0252921100069165 Published online by Cambridge University Press

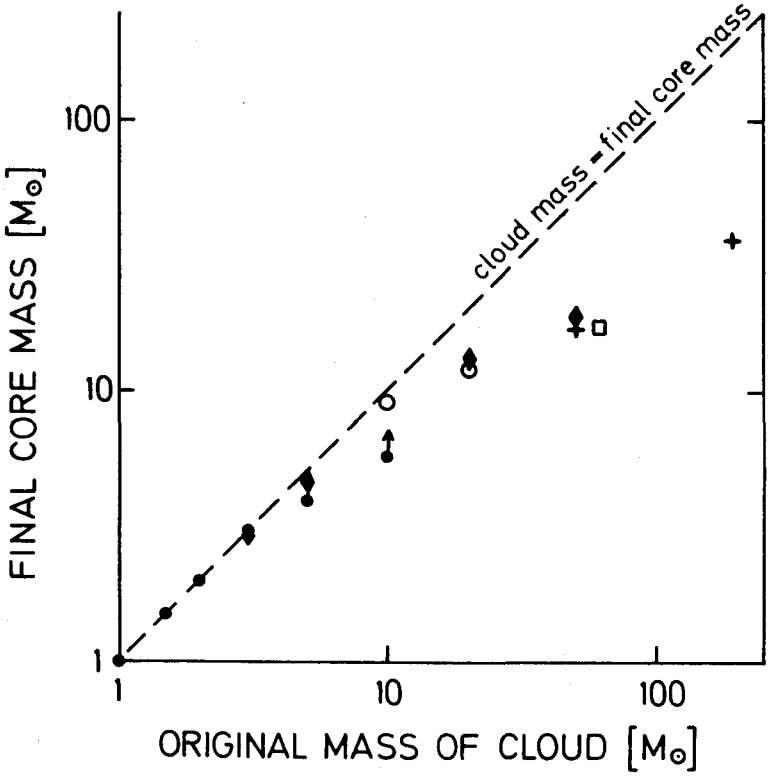

Fig.2. The results of calculations of the spherical collapse of protostellar clouds by several different authors is displayed together on a plot of the "initial cloud mass" versus "final mass of the core". The results of Larson (1972b) are denoted by filled circles (●), Westerbrook and Tarter (1975) by filled diamonds (◆), Appenzeller and Tscharnuter (1974) by an open square (□), Yorke and Krügel (1977) by crosses (+). Note that the formation of massive protostars is less efficient and the corresponding points therefore fall far below the dashed line for which the initial cloud mass is equal to the final mass of the resulting star.

https://doi.org/10.1017/S0252921100069165 Published online by Cambridge University Press

of energy when nuclear burning starts, if the core cannot adjust itself thermally fast enough. The overproduction of energy would lead to overheating and rapid expansion of the outer layers of the core. In the 60 $M_\odot$ protostellar calculation of Appenzeller and Tscharnuter only 16 $M_\odot$ remained in the core. The rest of the core and the envelope were blown off. By constructing steady-state solutions of the accretion envelope, Kahn (1974) concluded that radiation pressure should become important for massive protostars. Kahn was able to derive an expression for the upper mass limit for spherical accretion which depends on atomic constants and the properties of dust grains only. Larson and Starrfield (1971) estimated that the most important accretion limiting effect for an O star in the range 30 - 60 $M_\odot$ would be the ionization of the envelope. In a detailed numerical calculation of the dynamics of protostellar envelopes Yorke and Krügel (1977) found that an increasing fraction of the envelope is blown off by radiative acceleration on dust grains as one considers higher protostellar masses. Thus, the efficiency of converting protostellar cloud material into stars decreases for more massive stars; a 50 $M_\odot$ protostellar cloud produces a 16 $M_\odot$ star (32 % efficiency), whereas a 150 $M_\odot$ cloud is necessary to produce a 36 $M_\odot$ O star (24 % efficiency).

In Figure 2 the results of several authors is displayed in a plot of the initial protostellar cloud mass versus final mass of star. If all of the material in the protostellar cloud could fall onto the core, each point should lie on the dashed line as indicated. That this is not the case, especially for the more massive protostars, is clearly indicated. The 5 $M_\odot$ and 10 $M_\odot$ cases presented by Larson (1972b) represent lower limits to the final core mass, because the numerical calculations were stopped once hydrogen burning started.

3. The observable objects which are associated with massive protostars differ from those associated with low mass protostars. Due to their higher luminosity and their larger fraction of hydrogen-ionizing radiation, the massive protostars can be associated with "hot spots" of enhanced molecular radiation, masers, luminous infrared sources and compact HII regions. The low mass protostar, however, are to be associated with weak near infrared sources during the evolutionary stages in which they are obscurred optically, and with T Tauri and YY Orionis stars when they become optically visible. It is not clear whether masering spots can also be associated with low mass protostars, because too little is known about the pumping

mechanisms for such masers.

4. Finally, as suggested by Mezger (1977), the conditions favourable to the formation of massive protostars as opposed to low mass protostars may differ so greatly that the two would form in different regions or at different times. After comparison with Salpeter's initial mass function, Mezger interpretes the observed mass function in open clusters and subgroups of OB associations and the derived birth rate function as follows. Low mass stars ($M \leq 1\ M_{\odot}$) form continuously throughout molecular cloud complexes, whereas massive protostars can form only under very special conditions, such as under the influence of a sudden compression of the gas in a density wave shock. Observed T-Tauri associations would be an example of the formation of low-mass protostars only.

b.) Grain properties.

Before one can solve the equation of radiation transfer in the envelopes around protostars, it is necessary to specify the properties of the absorbing material. Although a lot of information on the extinction properties of the interstellar medium exists in the form of detailed extinction curves for a number of stars, ranging from infrared to ultraviolet frequencies, it has proved difficult to extract specific information about the nature of the dust grains responsible for this extinction. It seems likely, however, that the interstellar dust is not homogeneous in composition or size; more than one type of grain contributes to the extinction (Aannestad and Purcell, 1973). The $\lambda = 2200$ Å bump is commonly attributed to small graphite particles; the $\lambda = 10\mu$ absorption feature to silicate grains. However, it is not possible to explain all of the extinction properties of the interstellar medium with just a mixture of graphites and silicates (Bedijn, 1977). The most common explanation is the presence of volatile materials which accrete onto the surfaces of graphite and silicate grains. The chemical composition of this material is not clear. In the dense clouds associated with star formation, the condensation of more than one type of molecule onto the grains seems likely. Here the grains are for the most part well shielded from the various destructive influences such as cosmic rays and "hard" radiation (optical and ultraviolet starlight). In the following, we shall refer to the hypothesized mantel material as "ice", even though frozen H_2O may not be the main constituent.

https://doi.org/10.1017/S0252921100069165 Published online by Cambridge University Press

c.) Qualitative Structure of the Envelope.

From the results of Yorke and Krügel (1977) we deduce the structure of the protostellar cloud during the accretion phase, shown schematically in Figure 3. The approximate sizes of the various regions is indicated (in cm) for a 20 $M_\odot$ cloud after about one half of the mass has accreted onto the core. The central core has evolved to the point at which hydrogen-burning starts. The core is surrounded by the accretion shock front, where the freely falling material is decelerated to almost zero velocity, its kinetic energy being transformed into heat. In the immediate vicinity of the core and accretion shock front the optical and ultraviolet radiation field is much too intense for dust grains to survive, and out to a radius of about 10^{14} cm the gas is dust-free (and essentially opacity-free). Beyond the dust melting radius the radiation field has become sufficiently diluted geometrically, so that the more refractory grains, graphites and silicates, can survive. In a thin transition region just outside the dust melting radius the optical and ultraviolet radiation from the core is completely absorbed and reradiated in the infrared. Thus, the infalling dusty envelope acts as a false photosphere. The object appears to be an infrared source of temperature of about $T \sim 1000$ K.

The infrared radiation field in the envelope is still too intense for the more volatile materials, the ice mantels, out to a radius of about 10^{16} cm or larger. Outside this radius, the dust should be of a composition typical for cool, dense molecular clouds. In the inner regions of the cloud, where gravity is the dominant force, the density varies roughly as $r^{-3/2}$ and the velocity as $r^{-1/2}$. An exception to this may occur at the melting radius of dust, where in a thin transition region the "hard" radiation from the core and accretion shock could slow down and perhaps even reverse the inward flow of matter. This should happen in massive protostellar envelopes only, when the luminosity to mass ratio is large. In the outer regions of the cloud, the density distribution could very greatly from a $r^{-3/2}$ dependence, especially for massive clouds, where again radiative acceleration becomes important. Here, the larger grain radii due to the presence of mantels makes the dust a more efficient absorber of infrared radiation. But even for low mass protostars the density distribution in the outer regions may have nothing to do with a $r^{-3/2}$ law. One expects the density to merge gradually into the clumpy background of the larger cloud out of which the protostar had fragmented.

With this qualitative picture in mind, one can construct models of observed "protostars" with some degree of success. In general one

https://doi.org/10.1017/S0252921100069165 Published online by Cambridge University Press

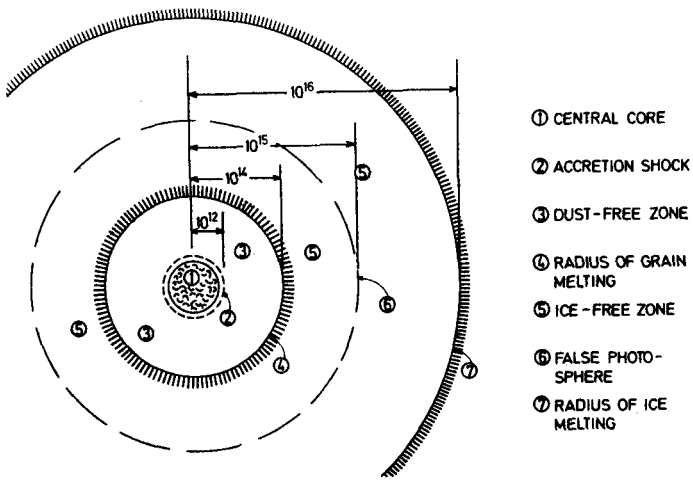

Fig. 3. Schematic representation of the structure of a collapsing protostellar cloud after the formation of a central (accreting) core (see text).

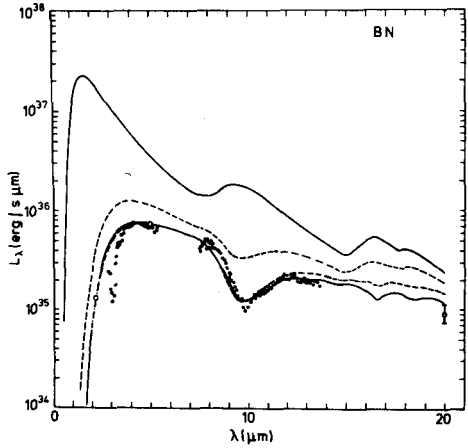

Fig. 4. Two possible model fits of the measured near infrared flux from the BN object. The two top curves represent the spectra of radiation coming from the "false photosphere" (see text), whereas the two bottom curves take into account the foreground extinction. The results were taken from Bedijn (1977) by permission of author.

https://doi.org/10.1017/S0252921100069165 Published online by Cambridge University Press

has many parameters that can be adjusted to reproduce measured spectra, namely the optical properties of the grains and the density distribution of the absorbing material. Then, by solving the equations of radiative transfer and heat balance of the grains simultaneously, one can determine both the radiation field (i.e. the infrared spectrum) and the temperature distribution in a self-consistent manner.

By restricting himself to envelope density distributions of $r^{-3/2}$ only, Bedijn (1977) was able to model the λ = 2 to 20μ spectrum of several protostellar candidates. In Figure 4 we show an example of two such model fits of the point source in the Orion Molecular Cloud 1, first seen by Becklin and Neugebauer (1967) and since called the Becklin - Neugebauer object or BN object. The two upper curves represent the spectral distribution of photons that leave the "false photosphere", assuming two different combinations of envelope and source parameters. By then allowing for foreground extinction (which includes the effect that the outer cloud regions should have in this wavelength range), the two lower spectra were obtained, which match closely the measured data. In this calculation Bedijn did not try to model the 3.1μ feature. Similar model spectra have also been presented by Finn and Simon (1977).

d.) Examples of evolutionary calculations of massive protostellar clouds (50 $M_\odot$ and 10 $M_\odot$).

An attempt to extend the observation of BN type sources into the far infrared, λ = 50μ - 200μ, has usually failed due to confusion with other far infrared sources. These BN sources are embedded in molecular clouds which often contain several compact HII regions, which are also strong emitters of far infrared radiation. At present the best possible angular resolution at 100μ is about 20" to 30", whereas most BN type objects are located within 5" to 20" of other powerful far infrared sources.

Harvey et al. (1977) have recently presented a notable exception to the above: Located coincident to a near infrared, BN type object (studied in detail from λ= 1μ to 20μ by Blair et al. 1977) in Sharpless 140, Harvey et al. have found a single far infrared source, at wavelengths ranging from λ= 35μ to 175μ. The resulting double-peaked spectrum and scale size of S140 IR are quite similar to the predictions of structure (Yorke and Krügel, 1977) and spectral appearance (Yorke, 1977) of massive protostellar envelopes.

The fact that this BN type source is also a strong emitter in

https://doi.org/10.1017/S0252921100069165 Published online by Cambridge University Press

Table 1: Core and Envelope parameters of a collapsing 10 $M_\odot$ protostellar cloud at various evolutionary times.

model	Δt (yr)	M_{core} ($M_\odot$)	L ($L_\odot$)	$\dot{M}$ ($M_\odot$/yr)	A_V (mag.)
A	7 600	1.5	850	0.000 242	5 700
B	26 600	5.3	3 630	0.000 141	1 520
max L	45 000	7.1	7 710	0.000 072	650
C	106 000	9.1	5 540	0.000 014	133
D	169 000	9.5	4 960	0.000 001	3

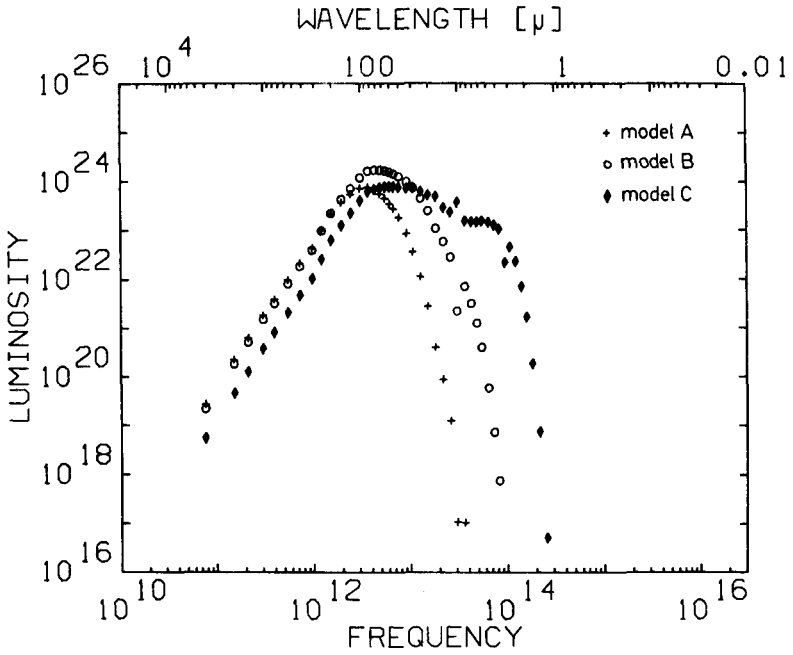

Fig. 5. The spectra from a collapsing 10 $M_\odot$ protostellar cloud during various evolutionary phases as described in table 1 and the text.

https://doi.org/10.1017/S0252921100069165 Published online by Cambridge University Press

the far infrared finds its natural explanation in figure 2. Massive protostellar clouds are inefficient producers of stars. Much of the material does not fall onto the central core; it is located in an expanding shell at several 10^{17} cm from the protostar. This shell absorbs part of the near infrared radiation coming from the "false photosphere" and reemits it in the far infrared.

What about the 10 $M_\odot$ case indicated in figure 2? Here, 95 % of the protostellar material did fall onto the protostar. What is its evolution and appearance?

In table 1 several important aspects of a recent numerical calculation of an evolving protostellar envelope are given. The age of the core after it was first formed Δt, the core mass M_{core}, total luminosity $L = L_{shock} + L_{core}$, the mass accretion rate of the core $\dot{M}$ and the total visual extinction A_v are given for several models during a calculated evolutionary sequence. These models are labeled A, B, max L (at which the maximum luminosity was attained), C and D. Model D was a compact HII region ($R_{HII} \sim 5 \times 10^{16}$ cm) and a powerful far infrared source. Without going into the details of these calculations at present, it should be noted that these calculations start from the initial collapse of a protostellar cloud and continue through the formation of an observable HII region. (The HII region was treated only approximately by always assuming ionization equilibrium.) In figure 5 we show the calculated spectra of models A, B and C. In model C the 10μ feature is even seen in emission. Only about 1000 years before model D did the ionization front leave the immediate vicinity of the accretion shock and travel as a weak R-type front through the surrounding envelope. This can be understood quantitatively if one considers the equilibrium size of a Strömgren sphere in a freely falling envelope. This can be easily calculated to be:

$$R_{HII} \approx R_{core} \exp\left\{\left(\frac{M_{core}}{[7\ M_\odot]}\right)\left(\frac{J}{[10^{47}\ s^{-1}]}\right)\left(\frac{\dot{M}}{[4\times10^{-6}\ M_\odot\ y^{-1}]}\right)^{-2}\right\} \quad (5)$$

where J is the number of ionizing photons emitted by the core and accretion shock in one second. For large accretion rates ($\dot{M} \gg 10^{-6}$ $M_\odot\ y^{-1}$), R_{HII} is necessarily close to the core, everything else remaining approximately constant. Every time $\dot{M}$ decreases by a factor of 2, R_{HII}/R_{core} is increased to the fourth power! When the inward flow of material is stopped and reversed in the outer layers of the cloud, the mass accretion rate at the surface of the core diminishes quickly, allowing the ionization front to propagate outwards rapidly.

https://doi.org/10.1017/S0252921100069165 Published online by Cambridge University Press

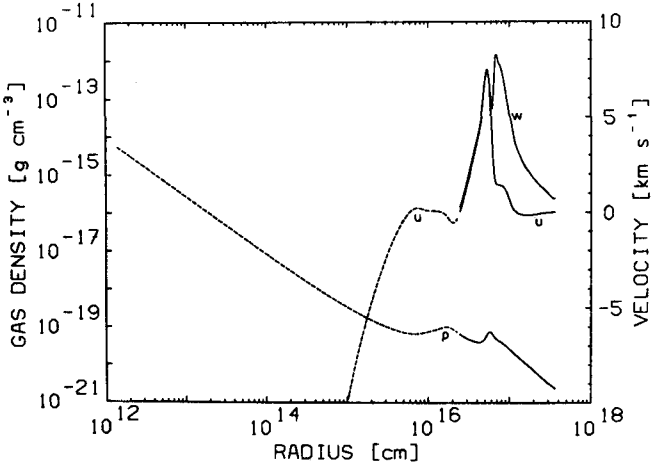

Fig. 6. The gas density ρ, the gas velocity u, and the mean velocity of the dust w are plotted versus the radius r in the 10 $M_\odot$ protostellar cloud at the evolutionary phase D (see table 1 and text). The parts of the cloud in which dust is depleted by 1000 with respect to the normal abundance is indicated by dashed lines.

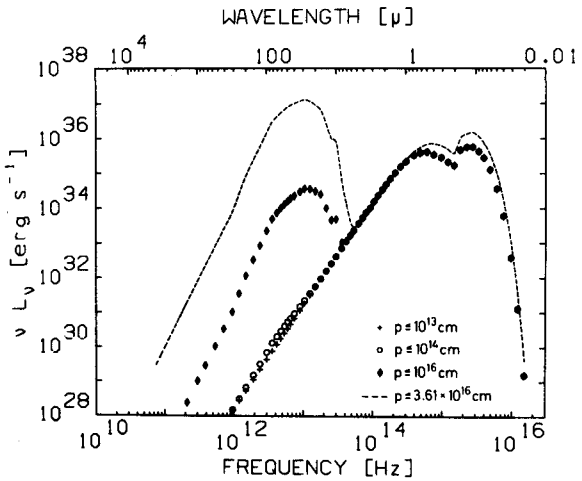

Fig.7. The expression $\nu L_\nu = \lambda L_\lambda$ of model D (see table 1 and text) is plotted as a function of frequency ν (and wavelength λ) as "seen" by "observers" using different "beam widths" p as indicated. The net theoretical spectrum from the entire disk $p \leq 3.61\ 10^{17}$ cm is given by the dashed curve.

https://doi.org/10.1017/S0252921100069165 Published online by Cambridge University Press

The velocity and density structure of the compact HII region are shown in figure 6. In the inner ionized regions the gas still has an $r^{-3/2}$ distribution ($r < 10^{15}$ cm) and the velocity is still roughly free fall, whereas further out in the cloud the density flattens and even increases. In these calculations the charge on the dust grains and the interaction between dust and gas is included when calculating the drift velocity of the dust through the gas. The size of the HII region is $\sim 5 \times 10^{16}$ cm. Outside the HII region, the drag forces of the (almost) neutral gas are small and the drift velocity of the dust is several km/s. Dust is being blown outwards. Inside the HII region the dust is essentially frozen into the gas - but depleted by a factor of 10. Inside about 2×10^{15} cm little dust is present, this having been swept clean by radiation pressure before the ionization front had been able to catch up to the outwardly moving dust.

The total spectrum νL_ν of the compact HII region (but not including the absorption and emission of the gas itself) is shown in figure 7. Here, the spectra are shown as seen by an "observer" using different "beam widths". From the expression $\nu L_\nu = \lambda L_\lambda$ one can directly compare the energy content at each frequency. One can easily see from figure 7 that about 10 times as much radiative energy is in the far infrared part of the spectrum as compared to the optical contribution, if one considers the radiation coming from the entire disk ($r = 3.6 \times 10^{16}$ cm). Using a smaller "beam size" and considering the radiation coming from the center of the disk only, one "sees" the optical part of the spectrum only. The 2200 Å feature is also observable in the spectra in figure 7. The spectral appearance depends on "beam size", because most of the far infrared radiation is produced in a dusty spherical shell outside of and in the outer parts of the compact HII region.

e.) *The spectral appearance of a 1 $M_\odot$ protostellar cloud.*

In figure 8 we show the spectra of a 1 $M_\odot$ collapsing cloud as calculated by Bertout (1976) at various evolutionary times. The core mass corresponding to each spectrum is indicated. After the formation of the hydrostatic core and embryo star of 0.03 $M_\odot$, the protostellar cloud emits most of its radiation in the near and far infrared, peaking at about $\lambda = 20\mu$. Later, when the central source first becomes visible optically, a double-peaked spectrum emerges, the optical radiation comes from the core and the near infrared from the surrounding envelope. Because of the approximate treatment of the shock front,

https://doi.org/10.1017/S0252921100069165 Published online by Cambridge University Press

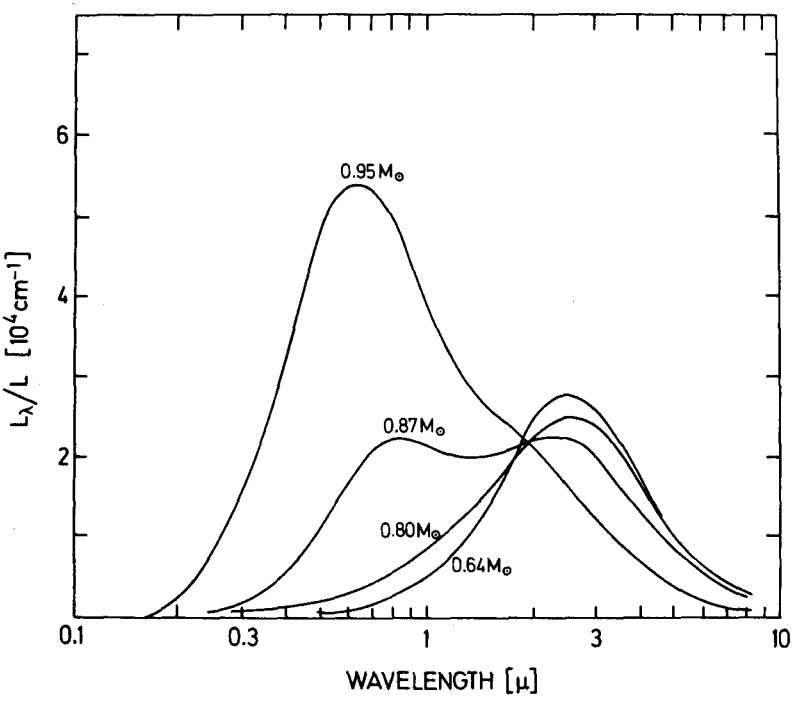

Fig.8. The spectra from a collapsing 1 $M_\odot$ protostellar cloud at various evolutionary times. The corresponding core mass at each time is indicated on the drawing. These spectra were taken from Bertout (1975) by permission of author.

https://doi.org/10.1017/S0252921100069165 Published online by Cambridge University Press

these spectra do not show the possible important contribution of the accretion shock and relaxation zone to the ultraviolet part of the spectrum (Ulrich, 1976). In spite of this shortcoming, these calculated continuum spectra qualitatively resemble the spectra of many T-Tauri stars.

But what about the formation of emission and absorption line profiles in the envelopes of protostars? It is unclear at present, whether the observed optical line profiles can at all be explained by a purely infalling envelope. In the case of YY Orionis stars, Bertout (1977) has shown that many features of the profiles can be explained by a spherically symmetric inflow of matter, but for T-Tauri emission line profiles, the conventional interpretation has been in terms of matter outflow. Strom et al. (1975) suggest that stellar winds can occur, which first clear out holes in the surrounding cloud material, thus allowing the protostars to illuminate or excite patches of gas. These patches of nebulosity would be observed as Herbig-Haro Objects.

Yet, the possibility of an inflow of material onto T-Tauri stars cannot be completely abandoned. Ulrich (1976), for instance, has shown that many features normally associated with mass outflow can in fact be explained by an infall model with rotation and emission from an accretion shock front. This view is supported by Lynden-Bell and Pringle (1974) who claim that most of the properties of T-Tauri stars can be explained by the evolution of accreting viscous disks.

III. The collapse of a rotating cloud

It has become apparent that many observed features of young, pre-main sequence stars cannot be explained by spherically symmetric collapse models alone. Furthermore, the existence of binary stars and planetary systems clearly indicates that rotation must play an important role in star formation. It is therefore not surprising that there has been an increasing interest in the evolution of rotating protostellar clouds. All numerical calculations relating to the evolution of rotating collapsing clouds (Larson, 1972a; Tscharnuter, 1975; Fricke et al., 1976; Black and Bodenheimer, 1976; Nakagawa, 1976) have the shortcoming that it has proved difficult (or impossible) to follow the evolution much beyond the earliest collapse stages. The nature of the problem requires one to use an implicit (iterative) numerical

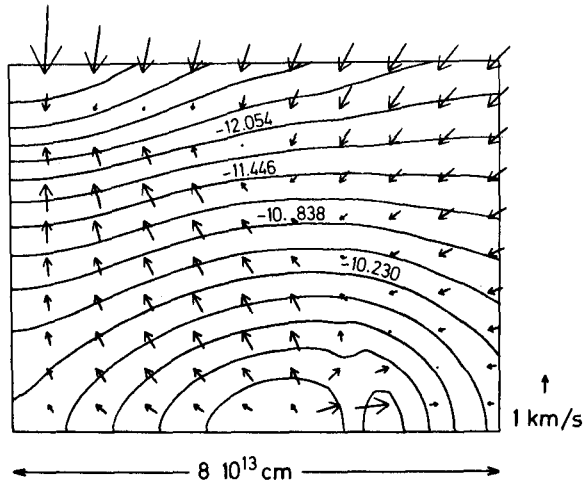

Fig.9. Density contours and velocity vectors for one quadrat of the central condensed regions of a collapsing and rotating 3 $M_\odot$ protostellar cloud, after the formation of a ring (see text). Values for logρ are as indicated.

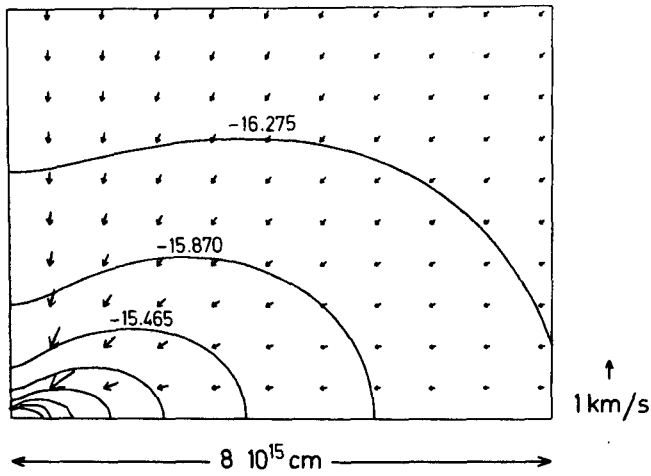

Fig.10. Same as figure 9, but a larger region is shown. The scale size has increased by a factor of 100 over the previous figure.

https://doi.org/10.1017/S0252921100069165 Published online by Cambridge University Press

technique in order to follow the hydrodynamical evolution of central condensations in the form of a core and/or a torus. Such a technique has been employed to date by Tscharnuter, 1975 and Fricke et al. 1976 only. Of course, all of these calculations require a large computer and are time-consuming as well as costly.

The early collapse proceeds in a similar non-homologous manner as encountered in the spherically symmetric calculations. Even if the angular velocity of rotation is so large that centrifugal forces balance the gravitational forces of attraction in the outer regions of the cloud, a small region of highly condensed material forms near the center, chiefly due to the infall of material with low angular momentum near the axis of rotation. The exact structure of the high density region, however, varies from author to author and depends sensitively both on the initial conditions and numerical details of the method used. If the initial total angular momentum of the cloud is low, however, a central optically thick core can form before the centrifugal force becomes important and the evolution of the cloud is qualitatively similar to the spherical case. The (flattened) hydrostatic core is surrounded by an accretion shock, which is stronger at the poles than at the equator. For values of the initial angular momentum higher than a critical value, the infall of material near the equator can be stopped and even reversed. The result is a flattened accretion disk, where a shock front forms at the poles only. In some calculations a torus or ring forms in the equatorial plane; in some cases it does not. According to recent calculations by Tscharnuter the formation of a ring becomes more likely, the higher the initial total angular momentum of the cloud. Until proven otherwise, it seems reasonable to assume that under some circumstances a "ring instability" can be excited, whereas for perhaps slightly different conditions the ring instability may be damped. If a ring forms it will invariably fragment, the result being a multiple system. As an example of the appearance of a rotating protostar we show preliminary results of numerical radiation transfer calculations being conducted by Tscharnuter and Yorke. The density and velocity structure of a 3 $M_\odot$ rotating protostellar cloud calculated by Tscharnuter in about 40 cpu hours on an IBM 360/91 is displayed in figures 9 and 10. In this cross sectional view the axis of rotation and symmetry is the left vertical axis. The equatorial plane which is assumed to be a plane of symmetry, is the lower horizontal axis. The contour lines depict lines of constant density. In figure 9 about 3 1/2 contour lines correspond to an order of magnitude change in the density. The scale of the drawing is

https://doi.org/10.1017/S0252921100069165 Published online by Cambridge University Press

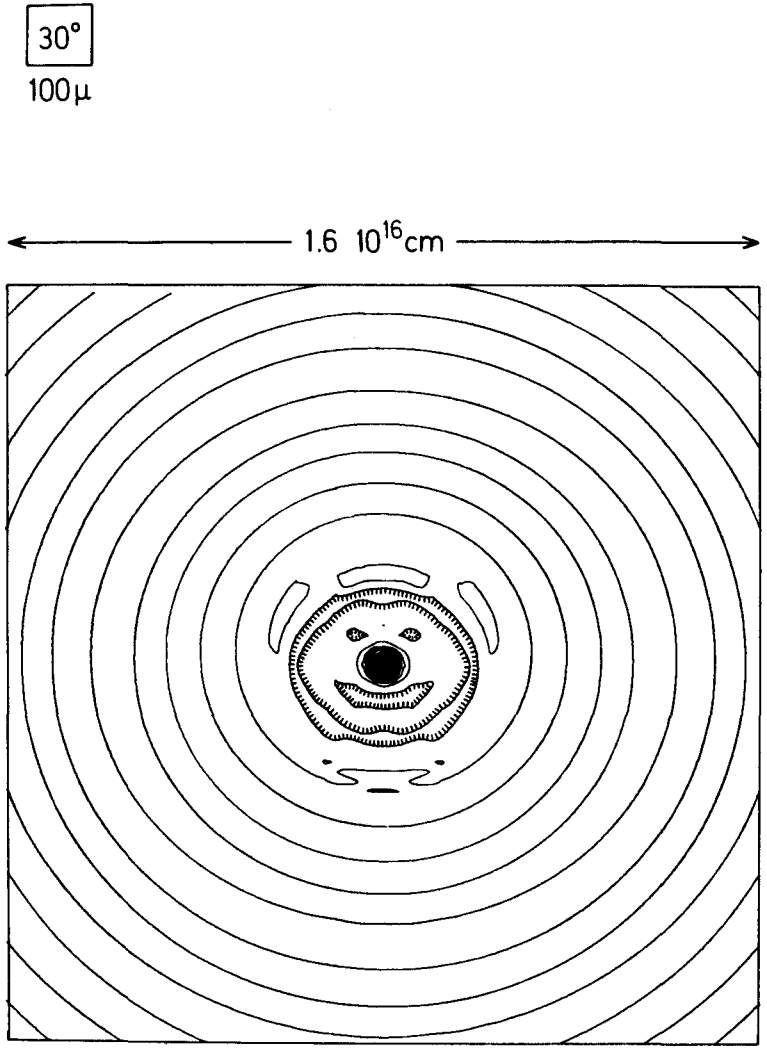

Fig. 11. Theoretical isophote contour map (lines of equal flux density) at 100μ from the 3 $M_\odot$ protostellar cloud described in text, "observed" at an inclination angle of 30°. Ten contour lines correspond to an order of magnitude, crossing three contour lines implies an increased flux density of a factor of 2. "Sinks" are indicated by countour lines with "teeth".

https://doi.org/10.1017/S0252921100069165 Published online by Cambridge University Press

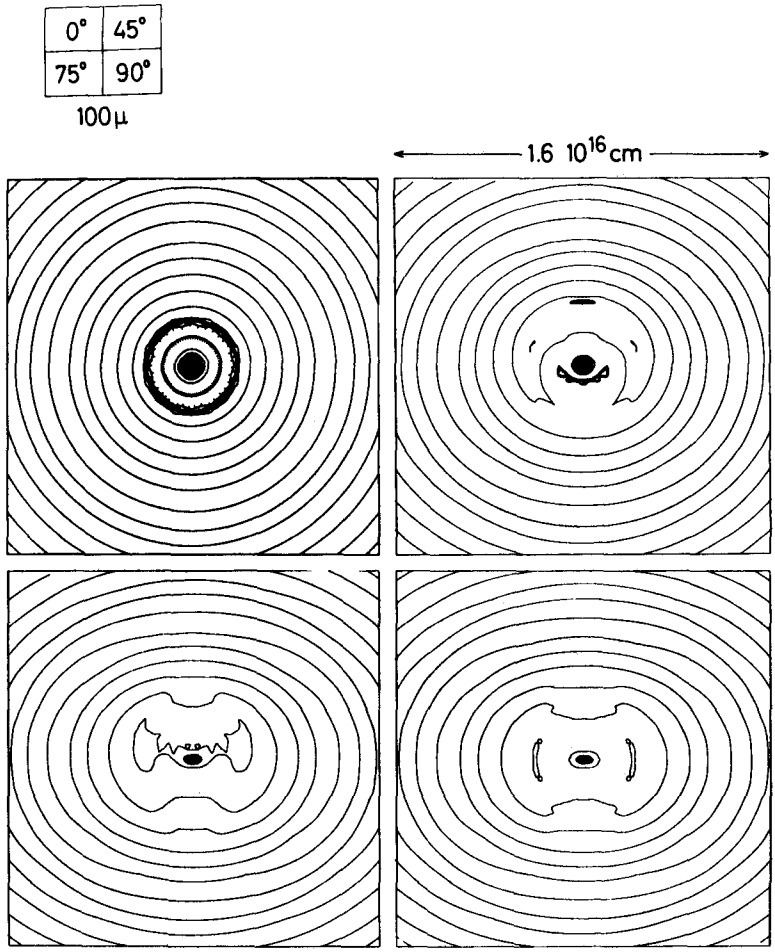

Fig. 12. Theoretical contour maps at 100μ, assuming different angles of inclination, 0° (pole-on). 45°, 75° and 90° (edge-on).

https://doi.org/10.1017/S0252921100069165 Published online by Cambridge University Press

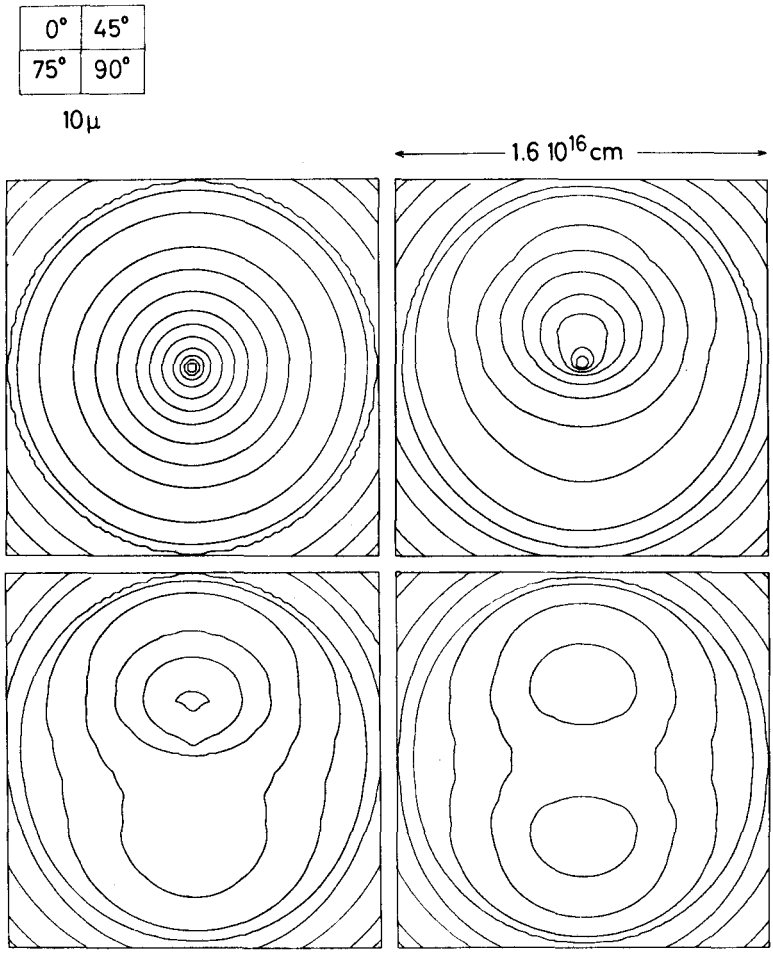

Fig. 13. Theoretical contour maps at 10μ, assuming different angles of inclination.

https://doi.org/10.1017/S0252921100069165 Published online by Cambridge University Press

$8x10^{13}$ cm along the equatorial plane by $6x10^{13}$ cm along the rotation axis. In figure 10 about 2 1/2 contour lines correspond to an order of magnitude change in density. The size scale is 100 times larger than the previous figure, $8x10^{15}$ cm by $6x10^{15}$ cm. The arrows indicate the direction and magnitude of the velocity, the scale for the velocity vectors is shown. In the upper part of figure 9 close to the axis of rotation the (smeared out) accretion shock front and relaxation zone is clearly indicated by a bunching of contour lines and by the rapid change in velocity. The shock strength decreases further from the axis. The structure of a dense ring is also shown. This picture is like a snap-shot taken at a particular instant of time. The ring is not stationary, but is expanding towards higher latitudes. In a somewhat larger scale (Figure 10) the flattened nature of the cloud is demonstrated.

Using the density and temperature distribution from Tscharnuter's calculations, it was possible to construct theoretical maps of this theoretical infrared source at various frequencies and angles of inclination. Some of the angles of inclination we used are indicated in figure 10. At 30^{o} and 100μ the resulting map is shown in figure 11 for the central area of size $1.6x10^{16}$ cm squared. Scanning the source from outside inwards we reach a local maximum of flux density at about $2x10^{15}$ cm. The density first falls, then rises again sharply at the center. The reason for the falloff is the melting of the grain mantels which is especially noticable in the far (100μ) infrared.

In figures 12 and 13 we present similar maps at 100 and 10μ respectively at inclination angles of 0^{o}, 45^{o}, 75^{o}, and 90^{o}. 0^{o} corresponds to a pole-on view and 90^{o} is an edge-on view. At 10μ the central source is visible only from pole-on to about 45^{o}. For larger angles of inclination only the heated dust above and below the equator is observed. The equator itself acts as an absorbing disk.

Acknowledgements: The author wishes to thank Drs. W. Tscharnuter and P. Bedijn for helpful and clarifying discussions and C. Rickl and R. Strasser for carefully typing the manuscript. For some of the new numerical results discussed here, the IBM 360/91 in Garching, Germany was used. Furthermore, the author thanks the organizers of the IAU Colloquium No. 42 for the invitation to the Bamberg meeting and for the kind hospitality extended to him there.

References

Aanestad, P.A., Purcell, E.M.: 1973, Ann. Rev. Astron. Astrophys. 11, 309
Appenzeller, I., Tscharnuter, W.: 1974, Astron. Astrophys. 30, 423
Becklin, E.E., Neugebauer, G.: 1967, Ap. J. 147, 799
Bedijn, P.J. 1977, Ph.D. Thesis, University of Leiden
Bertout, C.: 1976, Astron. Astrophys. 51, 101
Bertout, C.: 1977, Astron. Astrophys. 58, 153
Biermann, P., Kippenhahn, R., Tscharnuter, W., Yorke, H.: 1972, Astron. Astrophys. 19, 113
Black, D.C., Bodenheimer, P.: 1976, Astrophys. J. 206, 138
Blair, G.N., Evans, N.J., Van den Bout, P.A., Peters, W.L.: 1977 Astrophys. J., in press
Brown, R.L., Zuckerman, B.: 1975, Astrophys. J. Lett. 202, L125
Finn, G.D., Simon, T.: 1977, Astrophys. J. 212, 472
Fricke, K.J., Möllenhoff, C., Tscharnuter, W.: 1976, Astron. Astrophys. 47, 407
Harvey, R. M., Campbell, M.F., Hoffmann, W.F.: 1977, preprint
Kahn, F.D.: 1974, Astron. Astrophys. 37, 149
Kippenhahn, R., Tscharnuter, W.: 1975, Lec. Notes in Phys. 42, 79
Larson, R.B.: 1972a, Monthly Notices Roy. Astr. Soc. 156, 437
Larson, R.B.: 1972b, Monthly Notices Roy. Astr. Soc. 157, 121
Larson, R.B.: 1973, Ann. Rev. Astron. Astrophys. 11, 219
Larson, R.B.: 1977, in IAU Symposium No 75, "Star Formation", Ed. T. de Jong and A. Maeder, in press
Larson, R.B., Starrfield, S.: 1971, Astron. Astrophys. 13, 190
Lin, C.C.: 1971 in Highlights of Astronomy, Vol. II, p. 81
Lynden-Bell, D., Pringle, J.E.: 1974, Monthly Notices Roy. Astr. Soc. 168, 603
Mezger, P.G.: 1977, lecture presented at the Erice Summer School on "Infrared Astronomy", held in Erice, Sicily
Nakazawa, K., Hayashi, C., Takahara, M.: 1976, preprint
Shu, F.H., Milione, V., Gebel, W., Yuan, C., Goldsmith, D.W., Roberts, W.S.: 1972, Astrophys. J. 173, 557
Strom, S.E., Strom, S.E., Grasdalen, G.L.: 1975, Ann. Rev. Astron. Astrophys. 13, 187
Tscharnuter, W.: 1975, Astron. Astrophys. 39, 207
Tscharnuter, W.: 1976, Computer Physics Communications 12, 1
Ulrich, R.K.: 1976, Astrophys. J. 210, 377
Westbrook, C.K., Tarter, C.B.: 1975, Astrophys. J. 200, 48
Winkler, K.-H.: 1977, Ph.D. Thesis, Univ. Göttingen
Wynn-Williams, C.G., Becklin, E.E.: 1974, Publ. Astron. Soc. Pacific 85, 5
Yorke, H.W.: 1977, Astron. Astrophys. 58, 423
Yorke, H.W., Krügel, E.: 1977, Astron. Astrophys. 54, 183

D I S C U S S I O N of paper by YORKE:

KRAFT: How does the upper mass-limit change with Y (helium) and Z (metals)?

YORKE: I do not know how the upper mass limit should depend on Y. For a possible dependance on Z I refer again to Kahn's (1974) paper and my own numerical calculations. Kahn derived an expression for the upper mass limit, under the assumption that when steady-state spherical accretion is no longer possible due to the effect of radiative acceleration on the grains, a star cannot grow in mass. The net effect was that a higher Z implies a greater influence of dust grains and thus a lower upper-mass-

limit. This has important consequences with respect to the initial mass function as a function of the age of the Galaxy and therefore, with respect to galactic evolution in general.

GAHM: Cohen and Kuhi have found a number of stars in the Cep IV association. They are of late-type and very luminous. The visual absorption is small. Do the present accretion models account for this situation?

YORKE: I do not know.

DZIEMBOWSKI: The problem that worries me about dynamical calculations is the presence of instabilities in the case of negligible pressure.

YORKE: By assuming spherical symmetry one "forces" the material to move radially and only one "fragment" can occur at the center of the cloud. In axially symmetric calculations one can see if any fragmentation is taking place; if so, then rings should occur, as the only manifestation possible of a gravitational instability. In non-rotating axially symmetric calculations conducted by Larson in 1972, he did not find any rings in models with the same initial conditions as his earlier spherical calculations. Also, Tscharnuter (1975) did not find any rings in slowly rotating clouds - although such rings have occurred in the calculations by a number of authors of faster rotating clouds. The 3-D calculations to date are quite crude and inconclusive.

One should note that all these calculations include pressure.

DE LOORE: 1. You have shown a diagram relating the cloud mass and the final core mass, and you have told that a 150 $M_\odot$ cloud generates only a 36 $M_\odot$ star. Can you derive an upper limit for the stellar mass?

2. For the evolution of a 10 $M_\odot$ cloud you take into account accretion. Are these net accretion rates or are there also included losses of matter by stellar winds?

YORKE: 1. This diagram of initial protostellar cloud mass versus final mass of the star is certainly suggestive that the process of star formation becomes less efficient as one considers higher stellar masses. The fact that the results from all authors fit well in this qualitative interpretation - even though the details of their calculation varied widely - lends some support to this hypothesis. It is not possible to extrapolate the results to a "turnover", that is, an absolute upper mass limit of stars. The results of Kahn (1974), who calculated the largest accretion rates possible in an infalling, steady-state, absorbing envelope, show that for masses larger than about 60 $M_\odot$ no steady-state accretion is possible.

2. The accretion rates for the 10 $M_\odot$ protostellar clouds are the result of mass infall only. Mass loss from stellar winds was not taken into account. Stellar winds could become important during the late stages of the calculation only - simply because of the high density and high ram pressure of the infalling material. Because the free-fall velocity at the stellar surface is also the escape velocity, one can directly compare accretion rates with a hypothesized mass outflow of say 10^{-6} $M_\odot$/yr to see that a stellar wind will not stand a chance, until the late stages.

https://doi.org/10.1017/S0252921100069165 Published online by Cambridge University Press

STEPIEN: Did you include turbulence in your computations, and if not, don't you think that there can be profound changes in the presented picture if you include it?

YORKE: No, turbulence was not included in the spherical computations and I do not expect profound changes in the qualitative evolution. In Tscharnuter's hydrodynamic calculations, turbulence is included in the energy equation and the equation of angular momentum transfer in the following sense. Without any angular momentum transfer one has difficulty forming stars in a rotating cloud with too much angular momentum. This "angular momentum problem" can be exemplified if one considers the fact that in our solar system, even though the greatest fraction of the mass is in the sun, it only contains a small fraction of the angular momentum. How was the angular momentum transferred out of the central regions? Tscharnuter has included in his code a term allowing for the transfer of angular momentum, which in the results I showed had not yet become important. Of course the importance of this term is sensitive to the amount of viscous turbulence assumed.

SHERWOOD: 1. Why do you say that the BN object is pre-MS and not post-MS?

2. Don't your calculations describe equally well the OH/IR source OH 26.5 + 0.6 believed to be a Mira type LPV?

YORKE: 1. I never did claim that the BN object was pre-main sequence. If it is a young object then I claim it would have to be a hydrogen-burning star with an almost free-fall envelope. The excellent model fits by P.J. Bedijn (1977) assuming a free-fall envelope is suggestive but certainly not conclusive.

2. Perhaps. The radiative transfer calculations in the IR continuum depend only on the distribution of absorbing material around a central source (and of course on assumed grain properties), and not on the velocity field. It is possible that different type objects have similar IR continuum spectra.

https://doi.org/10.1017/S0252921100069165 Published online by Cambridge University Press